

RecQ helicase translocates along single-stranded DNA with a moderate processivity and tight mechanochemical coupling

Kata Sarlós, Máté Gyimesi, and Mihály Kovács¹

Department of Biochemistry, Eötvös Loránd University - Hungarian Academy of Sciences, "Momentum" Motor Enzymology Research Group, Eötvös Loránd University, H-1117, Budapest, Hungary

Edited* by Stephen C. Kowalczykowski, University of California, Davis, CA, and approved May 8, 2012 (received for review September 2, 2011)

Maintenance of genome integrity is the major biological role of RecQ-family helicases via their participation in homologous recombination (HR)-mediated DNA repair processes. RecQ helicases exert their functions by using the free energy of ATP hydrolysis for mechanical movement along DNA tracks (translocation). In addition to the importance of translocation per se in recombination processes, knowledge of its mechanism is necessary for the understanding of more complex translocation-based activities, including nucleoprotein displacement, strand separation (unwinding), and branch migration. Here, we report the key properties of the ssDNA translocation mechanism of *Escherichia coli* RecQ helicase, the prototype of the RecQ family. We monitored the pre-steady-state kinetics of ATP hydrolysis by RecQ and the dissociation of the enzyme from ssDNA during single-round translocation. We also gained information on the translocation mechanism from the ssDNA length dependence of the steady-state ssDNA-activated ATPase activity. We show that RecQ occludes 18 ± 2 nt on ssDNA during translocation. The hydrolysis of ATP is noncooperative in the presence of ssDNA, indicating that RecQ active sites work independently during translocation. In the applied conditions, the enzyme hydrolyzes 35 ± 4 ATP molecules per second during ssDNA translocation. RecQ translocates at a moderate processivity, with a mean run length of 100–320 nt on ssDNA. The determined tight mechanochemical coupling of 1.1 ± 0.2 ATP consumed per nucleotide traveled indicates an inchworm-type mechanism.

Helicases are NTP-driven nucleic acid motors that couple the liberation of chemical energy to mechanical movement along nucleic acid strands to exert diverse biological activities. *Escherichia coli* RecQ helicase is the prototype of its family [belonging to superfamily (SF) 2], whose members are essential in genome maintenance from bacteria to humans (1–3) by playing roles in homologous recombination (HR)-mediated dsDNA break (DSB) repair (4–7). In humans, loss-of-function mutations of at least three RecQ helicase homologs are linked to diseases (mostly Bloom, Werner, and Rothmund-Thomson syndromes), which are generally characterized by genome instability resulting in cancer predisposition and premature aging (8). *E. coli* RecQ suppresses illegitimate recombination (9) and regulates HR-mediated DSB repair via initiating HR and processing HR intermediates (2). Moreover, RecQ stabilizes stalled replication forks as part of the RecF pathway (10, 11).

Different types of translocation mechanisms were proposed for SF1 and SF2 helicases. An inchworm mechanism was proposed for bacterial PcrA (12, 13), UvrD (14), and human RecQ-family Bloom syndrome (BLM) (15) helicases, which perform unidirectional translocation based on the consumption of one ATP per kinetic cycle (dictated by a single rate-limiting step), leading to a single nucleotide translocation along ssDNA. A more complex, nonuniform inchworm stepping mechanism was suggested for UvrD (16), NS3 (17), and RecBCD (18) helicases. In this model, multiple rapid ATP hydrolysis-coupled translocation steps occur during a single kinetic cycle between two successive rate-limiting steps. A Brownian ratchet mechanism,

characterized by diffusion along the DNA strand in alternating weak and strong binding states, was used to describe the translocation of hepatitis C virus NS3 helicase (19). Because of the low coupling between the enzymatic (ATPase) and mechanical (translocation) cycles, ratchet mechanisms usually lead to the consumption of more than one ATP molecule per nucleotide traveled. In contrast to the above enzymes, although the biological functions of *E. coli* RecQ are well described (20–23), mechanistic knowledge of the underlying molecular processes is scarce.

DNA activates the ATPase activity of RecQ, and the ATP hydrolysis cycle is coupled to DNA unwinding (22, 24). DNA unwinding by RecQ is driven by translocation along the track strand in a 3'-to-5' direction (2, 22). Recent studies on the working mechanism of RecQ focused on its unwinding activity (25–27). Here, we report the key parameters of the translocation mechanism of RecQ (Fig. 1). ssDNA enhances the ATPase activity of RecQ in a length-dependent manner, which allows the extraction of mechanistic information from steady-state and transient profiles of translocation-coupled ATP consumption. We show that RecQ binding occludes about 18 ± 2 nt on ssDNA. Translocation is performed at a cycling rate of 35 ± 4 s⁻¹ with a mechanochemical coupling of 1.1 ± 0.2 ATP consumed per nucleotide traveled. RecQ translocates along ssDNA with a moderate processivity, performing a mean of 110–350 ATPase cycles while traveling 100–320 nt along ssDNA in a single run, as determined in different conditions. Mechanistic insights into the translocation mechanism will aid the understanding of translocation-based activities, including dsDNA unwinding, branch migration, nucleoprotein displacement, replication fork restart, HR regulation, and catenation.

Results

RecQ Active Sites Work Independently both in the Absence and Presence of ssDNA.

We measured the ATP concentration dependence of the steady-state ATPase activity of RecQ by using a pyruvate kinase-lactate dehydrogenase (PK-LDH)-linked enzyme assay both in the absence and presence of thymidine oligonucleotide of 54-nt length (dT₅₄) (Fig. S1). Based on Hill analysis, RecQ showed no cooperativity [the Hill coefficient (*n*) was 1.2 ± 0.2 and 1.0 ± 0.1 in the absence and presence of dT₅₄, respectively]. These data suggest that RecQ active sites work independently in these conditions. The steady-state *K*_{ATP} (Michaelis constant for ATP) and saturating DNA concentration (*k*_{cat}) data were in line with previous results (28, 29) (Fig. S1).

Author contributions: K.S., M.G., and M.K. designed research; K.S. performed research; K.S., M.G., and M.K. analyzed data; and K.S., M.G., and M.K. wrote the paper.

The authors declare no conflict of interest.

*This Direct Submission article had a prearranged editor.

Freely available online through the PNAS open access option.

¹To whom correspondence should be addressed. E-mail: kovacsm@elite.hu.

This article contains supporting information online at www.pnas.org/lookup/suppl/doi:10.1073/pnas.1114468109/-DCSupplemental.

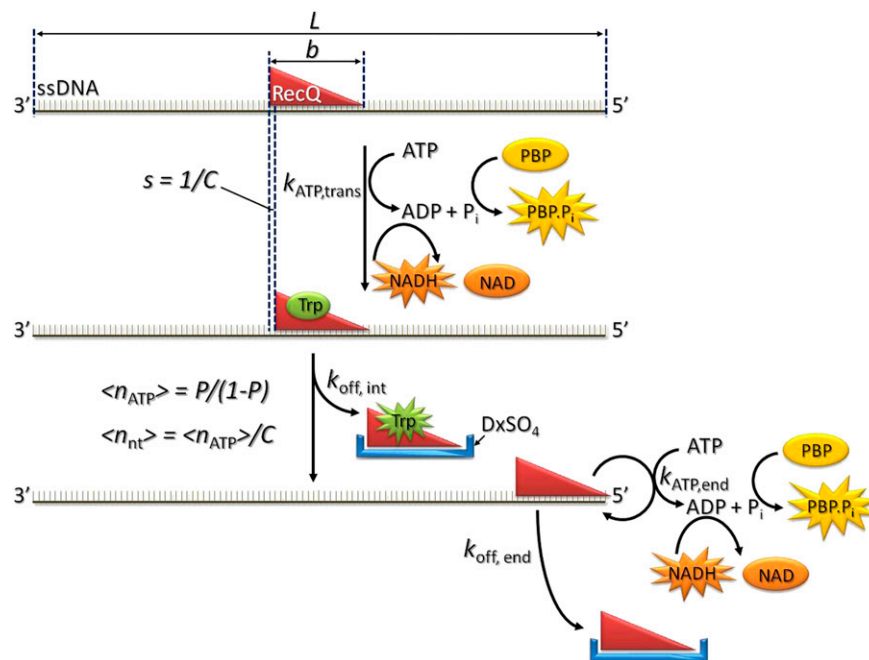


Fig. 1. Model for RecQ translocation along ssDNA. (Top) RecQ (red triangle) binds to an ssDNA strand of track length L (expressed in nucleotides) and occludes a site of b nucleotides in length. (Middle) On ATP-driven translocation, the enzyme travels s nucleotides per ATP molecule consumed, defining the mechanochemical coupling ratio C ($= 1/s$; number of ATP molecules hydrolyzed per nucleotide traveled). RecQ performs ATPase activities of $k_{ATP,trans}$ and $k_{ATP,end}$ during translocation and on reaching the end of the DNA track, respectively. Processivity, expressed as the probability of performing the oncoming ATP-consuming translocation cycle as opposed to dissociation, is defined as $P = k_{ATP,trans}/(k_{ATP,trans} + k_{off,int})$. The mean number of ATP molecules hydrolyzed (single-round ATP consumption amplitude) and nucleotides traveled (run length) in a processive run will thus be $\langle n_{ATP} \rangle = P/(1 - P)$ and $\langle n_{nt} \rangle = \langle n_{ATP} \rangle/C$, respectively (15, 30, 31). In this study, we determined the above-mentioned parameters by using optical signals reporting the appearance of ATP hydrolysis products ADP (by NADH absorbance using a PK-LDH linked assay, orange) and P_i (by using a fluorescently labeled P_i binding protein, MDCC-PBP, yellow), as well as the intrinsic Trp fluorescence of the enzyme (green), which increases on dissociation from DNA. In single-round pre-steady-state experiments, we applied $DxSO_4$ (blue) as a protein trap to prevent rebinding of RecQ to DNA after finishing the first processive run on ATP addition.

Single-Round Translocation Experiments Reveal Moderate Processivity and Tight Mechanochemical Coupling. Precise monitoring of the pre-steady-state kinetics of ATP hydrolysis in single-round translocation conditions allows the determination of mechanistic parameters of translocation (Fig. 1). Single-round conditions can be achieved by using a protein trap that inhibits the rebinding of the enzyme to DNA after dissociation. As discussed earlier, the amplitude of ATP hydrolyzed during a processive run (moles of ATP hydrolyzed per mole of enzyme) is influenced by the length of the track (L), the length of the DNA stretch occluded by the enzyme (b), the processivity (P , expressed as the probability of the oncoming translocation step), and the number of ATP molecules hydrolyzed (c) and nucleotides traveled (m) in a translocation step (30, 31). Analysis of ATP hydrolysis profiles allows robust determination of the mechanochemical coupling ratio ($C = c/m$, number of ATP molecules hydrolyzed per nucleotide traveled), whereas c and m cannot be determined separately from such data (30, 31). Therefore, we earlier developed a method for the analysis of the track length dependence of ATP hydrolysis transients, which requires a small number of non-covariant floating parameters (30) (Eq. S1). Regardless of the potential complexity (nonuniformity) of the translocation mechanism, this analysis allows the robust determination of the most important macroscopic translocation parameters, including b , C , and the mean number of ATPase cycles performed in a processive run [$\langle n_{ATP} \rangle = P/(1 - P)$] as well as the mean processive run length [$\langle n_{nt} \rangle = P/(1 - P)/C$] (Fig. 1).

To monitor ATP hydrolysis during single-round ssDNA translocation by RecQ, we recorded transient kinetic profiles of phosphate (P_i) production from ATP in stopped-flow experiments

by using the fluorescent signal of a bacterial P_i binding protein (MDCC-PBP) (15, 30) (Fig. 2A). In these experiments we applied dextran sulfate ($DxSO_4$) as a protein trap to ensure single-round conditions. RecQ was preincubated with oligo-dT substrates of different length (Fig. 2A–C) or M13 phage circular ssDNA (Fig. 2C), and it was then rapidly mixed with ATP plus $DxSO_4$ in the stopped-flow apparatus. The time courses of the reaction showed two phases with a characteristic breakpoint, which marked the dissociation of the enzyme after a single translocation event. The first phase corresponded to ATP hydrolysis during translocation along ssDNA, whereas the second phase represented ATP hydrolysis in the trap-bound state (Fig. 2A).

Fig. 2B shows the oligo-dT length dependence of the amplitudes of P_i production (mol P_i /mol RecQ) during single-round translocation at different $DxSO_4$ concentrations. As can be inferred from Fig. 2B, the x intercept, initial slope, and maximal P_i production amplitude values reflect parameters b , C , and $\langle n_{ATP} \rangle$ [thus, $P = \langle n_{ATP} \rangle / (\langle n_{ATP} \rangle + 1)$], respectively (compare with Fig. 1 and Eq. S1). The fits yielded $b = 18 \pm 2$ nt and $C = 1.1 \pm 0.2$ ATP/nt. These values were independent of trap concentration (Fig. 2B and Table 1).

As reflected in the maximal P_i production amplitudes (Fig. 2B), processivity was significantly influenced by trap concentration, although the trap effect was less pronounced in M13 than in oligo-dT substrates (Fig. 2C). This can be attributed to the lack of end effects in M13 DNA. To determine the genuine (trap-free) translocation processivity of RecQ, we applied an equation we developed earlier for analysis of the dependence of $\langle n_{ATP} \rangle$ on trap concentration (30) (Fig. 2C and Eq. S2). Extrapolated trap-free $\langle n_{ATP} \rangle$ values were 110 in the case of various lengths

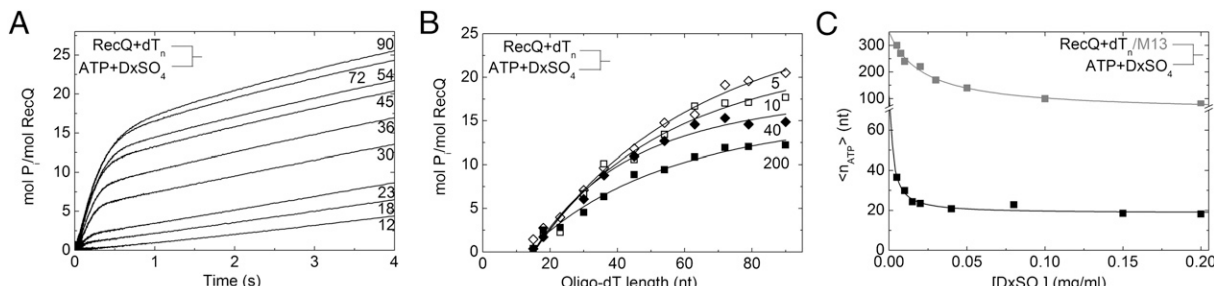


Fig. 2. Single-round translocation of RecQ along ssDNA. (A) Time courses of P_i production from ATP during translocation of RecQ along ssDNA substrates of different length ($dT_{12} - dT_{90}$, lengths in nucleotides indicated), which were recorded on mixing 25 nM RecQ plus 1 μ M thymidine oligonucleotides of various length (dT_n) with 0.5 mM ATP plus 0.04 mg/mL $DxSO_4$ in the stopped flow. P_i production was monitored by using the fluorescence change of MDCC-PBP (5 μ M in all syringes). (B) Oligo-dT length dependence of the corrected amplitudes of P_i production (mol P_i /mol RecQ) during the first phase, corresponding to translocation along ssDNA. Indicated values are $DxSO_4$ concentrations in (μ g/mL). Data were analyzed using Eq. S1. Data points were corrected based on Fig. S2B. (C) Dependence of the determined mean number of ATPase cycles performed in a processive run ($\langle n_{ATP} \rangle$; Fig. 1) on $DxSO_4$ concentration during translocation along linear oligo-dT (black) and circular M13 phage ssDNA (gray). Data points obtained with dT_n substrates at $DxSO_4$ concentrations enabling effective trapping (Fig. S2 A-E) were used in fits based on Eq. S2 (30) to determine the trap-free $\langle n_{ATP} \rangle$ values. Obtained parameters are listed in Table 1.

of thymidine oligonucleotides (dT_n) and 350 in M13, corresponding to processivity values of $P = 0.991$ and $P = 0.997$, respectively (Figs. 1 and 2C and Table 1). The mean processive run length ($\langle n_{nt} \rangle = \langle n_{ATP} \rangle / C$) was calculated to be 100–320 nt.

The reliability of processivity values extrapolated to zero trap concentration depends on the condition that the trapping efficiency is close to 100% even at the lower end of the applied trap concentration range. Trapping efficiency can be expressed in steady-state and pre-steady-state terms as the extent of inhibition of the DNA-activated ATPase activity of the helicase and the extent of suppression of the rapid P_i production amplitude, respectively. We determined the steady-state and pre-steady-state trapping efficiencies at various $DxSO_4$ concentrations (Fig. S2). These experiments revealed that data points recorded at and above 0.005 mg/mL $DxSO_4$ reliably report single-round translocation (Fig. S2). The $\langle n_{ATP} \rangle$ values shown in Fig. 2B were corrected based on the results of these control experiments (described in legend for Fig. S2E).

ssDNA Length Dependence of ATPase Activation Reveals Translocation Parameters. Previous studies by others (32) and us (15) have shown that the ssDNA length dependence of the steady-state parameters of the ssDNA-activated ATPase activity of helicases, namely, the ATPase activity at saturating DNA concentration (k_{cat}) and the DNA concentration required for half-maximal saturation of the ATPase activity (K_{DNA}) (an example for dT_{54} is provided in Fig. 3A), carries information on the translocation mechanism (Fig. 1 and Eq. S3). Therefore, we determined the

ssDNA length dependence of the steady-state ATPase activity of RecQ by using a PK-LDH coupled assay (Fig. 3). Similar to our recent observations on human BLM (15), the k_{cat} and K_{DNA} values of RecQ were greatly influenced by ssDNA length. The k_{cat} value stagnated up to 18 nt, then increased with oligo-dT length, and reached quasisaturation above 60 nt (Fig. 3B). For the analysis of the ssDNA length dependence of k_{cat} , we applied a function we developed earlier (Eq. S3) to reveal translocation parameters (15). The analysis revealed the ATPase rate constant during translocation ($k_{ATP,trans} = 35 \pm 4 \text{ s}^{-1}$), the ATPase rate constant at the end of the DNA track ($k_{ATP,end} = 14 \pm 2 \text{ s}^{-1}$), and the dissociation rate constant from the DNA end ($k_{off,end} = 4 \pm 1 \text{ s}^{-1}$) (Table 1). It also yielded the macroscopic step size ($s = 0.91 \pm 0.13 \text{ nt/ATP}$) and the DNA length occluded by the enzyme ($b = 18 \pm 2 \text{ nt}$) (Table 1). K_{DNA} values dramatically decreased with DNA length until about 23 nt (Fig. 3C), a value slightly larger than the b value of $18 \pm 2 \text{ nt}$ determined consistently from the ssDNA length dependence of P_i production amplitudes of Fig. 2B and that of the k_{cat} values of Fig. 3B (Table 1). However, the ssDNA length dependence of K_{DNA} allows only a qualitative analysis and provides an estimate for the upper limit of b .

The model applied for the analysis of the data of Fig. 3B (15) (Eq. S3) interprets the ssDNA length dependence of k_{cat} in the framework of two types of ATPase cycles performed by the enzyme: one exerted during translocation ($k_{ATP,trans}$) and a “futile” (nontranslocative) one occurring at the DNA end before dissociation ($k_{ATP,end}$) (Fig. 1 and Table 1). Alternative models have been proposed in which k_{cat} is influenced by a slow initiation

Table 1. Parameters of RecQ translocation along ssDNA

Parameter	Method of determination	Value
$k_{ATP,trans}$ (ATP hydrolysis rate constant during translocation, s^{-1})	PK-LDH assay	35 ± 4
$k_{ATP,end}$ (ATP hydrolysis rate constant at 5'-end, s^{-1})	PK-LDH assay	14 ± 2
$k_{off,int}$ (dissociation rate constant from internal sites on DNA, s^{-1})	Trp fluorescence	0.12 ± 0.01
$k_{off,end}$ (dissociation rate constant from 5'-end, s^{-1})	PK-LDH assay	4 ± 1
C (coupling stoichiometry, ATP hydrolyzed per nucleotide traveled, nt^{-1})	PK-LDH assay, MDCC-PBP	1.1 ± 0.2
s ($= 1/C$, nucleotide traveled per ATP hydrolyzed)	PK-LDH assay, MDCC-PBP	0.91 ± 0.13
b (occluded site size, nucleotides)	MDCC-PBP, PK-LDH assay	18 ± 2
k_t ($= k_{ATP,trans}/C$, translocation rate, nt/s)	PK-LDH assay, MDCC-PBP	31 ± 8
P (processivity, probability of taking the next translocation step)	Trp fluorescence	$27-43$
$\langle n_{ATP} \rangle$ [$= P/(1 - P)$, mean number of ATPase cycles performed in a single run]	MDCC-PBP, PK-LDH assay, Trp fluorescence	$0.991-0.997$
$\langle n_{nt} \rangle$ ($= \langle n_{ATP} \rangle / C$, mean processive run length, nucleotides)	MDCC-PBP, PK-LDH assay, Trp fluorescence	$110-350$
		$100-320$

The parameters of RecQ translocation along ssDNA provided in this table can be compared with those in Fig. 1.

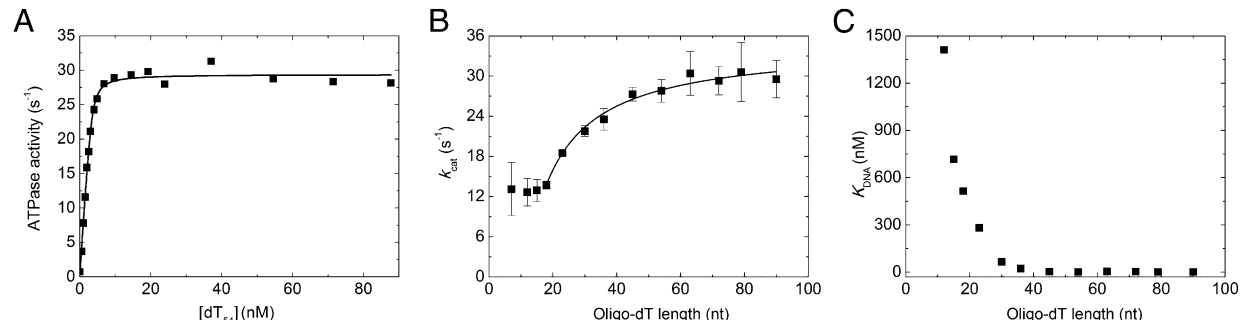


Fig. 3. ssDNA length dependence of RecQ ATPase activity. (A) dT₅₄ concentration dependence of the steady-state ATPase activity of RecQ. RecQ (15 nM) and ATP (1 mM) were titrated with increasing concentrations of dT₅₄ in a PK-LDH coupled assay. Fit to the data using a quadratic binding equation yielded $K_{DNA} = 1.8 \pm 0.1$ nM and $k_{cat} = 29 \pm 1$ s⁻¹ in the experiment shown. (B) Oligo-dT length dependence of k_{cat} values determined from oligo-dT concentration dependence of the steady-state ATPase activity of RecQ. The solid line shows a fit based on Eq. S3 (15). Obtained parameters are listed in Table 1. (C) Dependence of K_{DNA} values (oligo-dT concentrations required for half saturation of ATPase activity of 15 nM RecQ) on oligo-dT length.

process preceding translocation instead of ATPase cycling at the DNA end [e.g., by Fischer et al. (33) for the yeast Isw2 chromatin remodeling enzyme]. However, we found that the onset of ATP hydrolysis (as revealed by MDCC-PBP fluorescence) on rapid stopped-flow mixing of DNA-free RecQ and a premixture of dT₇₂ plus ATP was similar to that recorded on mixing a pre-formed RecQ-dT₇₂ complex with ATP and that no significant lag was observed in any case (Fig. S3). This finding rules out a significant effect of a slow initiation process on the measured steady-state k_{cat} values.

Analysis of steady-state ATPase rates calculated from MDCC-PBP fluorescence stopped-flow records (Fig. 2A) yielded parameters ($s = 1/C$ and b ; compare with Fig. 1) that were in accordance with those determined from the results of the PK-LDH coupled assay (Fig. 3 and Table 1). The $k_{ATP,trans}$ value of 35 ± 4 s⁻¹ and the coupling stoichiometry (C) of 1.1 ± 0.2 ATP/nt (Fig. 2B) define a macroscopic translocation rate ($k_t = k_{ATP,trans}/C$) of 31 ± 8 nt/s.

Tryptophan Fluorescence Measurements Verify the Mechanoenzymatic Parameters. The experiments of Figs. 2 and 3 used signals originating from RecQ's ATPase activity. These measurements rely on the determination of the concentration of active enzyme. To validate the translocation model by experiments whose analysis is independent of active enzyme concentration, we monitored the kinetics of RecQ dissociation from ssDNA during translocation by using the concomitant increase in tryptophan (Trp) fluorescence. As discussed by Fischer and Lohman (31), the DNA dissociation kinetics of an enzyme translocating along an infinite-length track will be governed by the dissociation rate constant

from internal sites ($k_{off,int}$), and will thus follow a single exponential time course. Therefore, we determined the DxD_{SO₄} concentration dependence of the observed rate constant (k_{obs}) of dissociation of translocating RecQ from internal sites of poly-dT, which can be considered a quasi-infinite length track (Fig. 4). Similar to an earlier work on UvrD (34), we determined the trap-free $k_{off,int}$ by linear extrapolation of k_{obs} to zero trap concentration (Fig. 4B). The $k_{off,int}$ value of 0.12 ± 0.01 s⁻¹ determined in these experiments and the $k_{ATP,trans}$ value of 35 ± 4 s⁻¹ determined in the PK-LDH experiments of Fig. 3B define a trap-free processivity of $P = k_{ATP,trans}/(k_{ATP,trans} + k_{off,int}) = 0.997$, which is consistent with the processivity values independently determined from the P_i production amplitudes in the experiments of Fig. 2. In control experiments performed at 0.1 mg/mL DxD_{SO₄} in the absence of ATP, k_{obs} values were about an order of magnitude higher than those obtained in the presence of ATP (1.8 s⁻¹ vs. 0.2 s⁻¹; Fig. 4B), indicating that the Trp fluorescence data obtained in poly-dT and ATP reliably report dissociation after single-round translocation.

To verify the macroscopic translocation rate (k_t , expressed in nt/s) calculated from the MDCC-PBP and PK-LDH results (Figs. 2 and 3), we determined the oligo-dT length dependence of Trp fluorescence transients on dissociation of RecQ from oligo-dT after single-round translocation (Fig. S4). Such experiments have been used to determine k_t by applying different analytical approaches (31, 35). The recorded time courses could be well fitted by single exponentials (Fig. S4A). Analysis of the oligo-dT length dependence of the observed DNA interaction lifetimes ($\tau_{obs} = 1/k_{obs}$) confirmed that k_t falls in the range of 27–

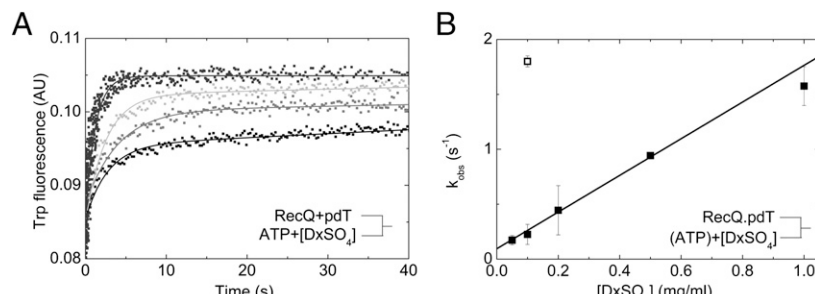


Fig. 4. Dissociation of RecQ from ssDNA during single-round translocation. (A) Time courses of dissociation of 0.5 μ M RecQ from 25 μ M (concentration in nucleotides) poly-dT (pdT) on mixing with 5 mM ATP plus varying concentrations of DxD_{SO₄} (Lower to Upper: 0.05, 0.1, 0.2, and 0.5 mg/mL), monitored by the Trp fluorescence change of RecQ. Solid lines show single exponential fits to the data. (B) DxD_{SO₄} concentration dependence of the observed rate constants (k_{obs}) of RecQ dissociation from pdT (experimental conditions were as in A; ■) or mixing RecQ plus pdT with 0.1 mg/mL DxD_{SO₄} in the absence of ATP (□). The intercept of the fitted linear indicated a trap-free dissociation rate constant ($k_{off,int}$) of 0.12 ± 0.01 s⁻¹ from internal ssDNA sites during translocation. AU, arbitrary units.

43 nt/s (Fig. S4B and Eq. S4), consistent with that determined based on the results of PK-LDH and MDCC-PBP experiments ($k_t = 31$ nt/s; Figs. 2 and 3 and Table 1).

Discussion

In this study, we describe the translocation of RecQ helicase along ssDNA based on a comprehensive set of steady-state and pre-steady-state experiments using three different types of signal (Fig. 1 and Table 1). We determined the key parameters of translocation, including the ATP hydrolysis rate constant during translocation ($k_{ATP,trans}$), the rate constants of dissociation of RecQ from internal sites on DNA ($k_{off,int}$) and from the 5'-end ($k_{off,end}$), the length of the DNA stretch occluded by the enzyme (b), the mechanochemical coupling stoichiometry (C), and the processivity (P) defining the mean processive run length (Table 1).

The analyses based on the DNA length dependence of P_i production during single-round translocation (Fig. 2), in line with the steady-state ATPase (Fig. 3) and DNA dissociation (Fig. 4) data, revealed that the mean processive run length ($\langle n_{nt} \rangle$) is between 100 and 320 nt (Table 1). Thus, the processivity of RecQ appears higher than that of human BLM, which takes around 50 steps on average (15), but is much lower than that of the very processive RecBCD complex, which takes several thousand steps (36). The translocation run length of RecQ is comparable to those reported for NS3 (37) and PcrA (38) helicases, traveling a mean of 200–300 nt during a single run.

RecQ helicase consumes one ATP per single nucleotide movement (Figs. 2 and 3 and Table 1), suggesting an inchworm mechanism for translocation. This behavior is similar to that previously reported for PcrA (13), UvrD (16), and BLM (15) helicases. Conserved amino acids of the so-called “aromatic-rich loop” located sequentially after motif II of the *N*-core RecA domain of RecQ have been shown to be important structural determinants of the tight coupling between ATP hydrolysis and translocation (29). We note that based on the available data, one cannot rule out the possibility of more complex kinetic mechanisms in which multiple ATPase cycles could occur within a global kinetic step characterized by a single rate-limiting event (31). Such scenarios could be detected by high signal-to-noise ratio data on translocation along fluorescently labeled ssDNA substrates, which we found unattainable in the case of RecQ, despite extensive trials using various fluorescent probes. Nevertheless, the parameters determined in this study remain valid to describe the key features of translocation even in the case of more complex kinetic behavior.

During translocation, RecQ exerts an ATPase cycling rate ($k_{ATP,trans}$) of 35 ± 4 s⁻¹ (Table 1). Together with the tight coupling stoichiometry ($C = 1.1 \pm 0.2$ ATP/nt), these values define a translocation rate ($k_t = k_{ATP,trans}/C$) of 31 ± 8 nt/s (confirmed by the DNA dissociation experiments in Fig. S4) similar to those of PcrA (38) and NS3 (37).

The DNA length dependence of the steady-state ATPase k_{cat} values, consistent with results of transient kinetic single-round translocation experiments, yielded an occluded site size of 18 ± 2 nt (Figs. 1–3 and Table 1). Qualitative analysis of the steady-state K_{DNA} values also supported this value (Fig. 3C). This value is somewhat larger than previously predicted (21, 25), although the accuracy of the previously applied methods was limited because fluorescence anisotropy titrations and mobility shift experiments were performed using a 3-kb plasmid.

The determined parameters (Fig. 1 and Table 1) suggest a translocation mechanism for RecQ similar to that of BLM, involving relatively rapid dissociation from the 5'-end, thereby avoiding extensive futile cycling. The translocation and unwinding activities of RecQ have also been investigated at the single-molecule level (39), resulting in $k_{ATP,trans}$ values similar to those determined in this study. This fortifies the theory that RecQ helicase unwinds dsDNA in an active manner.

The oligomeric state of RecQ during different activities has been widely discussed (23–27). In line with previous studies (28, 29), we observed no cooperativity in the steady-state ATPase activity of RecQ in the absence of DNA and in the presence of ssDNA (Fig. S1). This finding indicates that RecQ active sites work independently in these conditions, not excluding the possibility of oligomerization during dsDNA unwinding and the processing of complex DNA substrates. Studies on the unwinding activity of RecQ suggested that efficient dsDNA unwinding occurs in multimeric form (23, 26, 27). The phenomenon that ssDNA translocation is performed by monomers and dsDNA unwinding is performed by oligomers was observed in the case of other SF1 and SF2 helicases, including PcrA (38), UvrD (34, 40–42), Rep (43, 44), and NS3 (37), suggesting a role of oligomerization in the regulation of switching between different activities. Dynamic oligomerization was also reported for human WRN (45) and RecQ1 (46) helicases, suggesting the importance of substrate-induced oligomerization also in the case of RecQ-family helicases (47). Furthermore, oligomerization is likely to be influenced by solution conditions (e.g., temperature, ionic strength, pH). Therefore, the results of different studies need to be interpreted carefully, and the substrate-induced oligomerization of helicases provides grounds for future studies.

Recent studies of the ssDNA translocation mechanism of RecQ yielded mechanistic parameters that were different from the ones reported in the present work (48, 49). The lower k_t (14–26 nt/s) and, in turn, shorter processive run length (36 nt) (48) were determined at a lower temperature (20 °C) than that in the present work (25 °C). These parameters may also be influenced by the use of different protein traps (heparin vs. DxSO₄ in the present study). Compared with the present study, the larger occluded site size (30–34 nt) (48) and higher cooperativity in ATP hydrolysis during ssDNA translocation ($n = 2.1$) (49) can be attributed to a possible difference in the oligomeric state of the enzyme as a result of the lower ionic strength of the solution in those studies (48, 49). It should also be noted that the data analysis methods presented in this work are considerably different from those used in earlier studies.

RecQ-family helicases play roles in both the early and late stages of HR (4). RecQ works in concert with RecJ exonuclease to generate 3'-overhanged invading strands for homology search mediated by the RecA recombinase (10, 11). The processive action of RecQ may be important to generate ssDNA stretches of sufficient length for extended homology search to avoid illegitimate recombination. RecQ, SSB, and RecA cooperate in controlling the formation and disruption of HR intermediates (2). The suppression of illegitimate HR by RecQ (9) indicates its importance in the quality control of HR, which was also proposed as an important *in vivo* role for human BLM (50). The processivity of RecQ may also be important for RecQ- and RecJ-mediated processing of stalled replication forks (3). All these activities require a moderate processivity, which indicates the physiological relevance of our findings. The results presented in this work provide insights into the molecular process of ssDNA translocation, and thus aid the understanding of more complex biological activities of RecQ, including DNA unwinding and the disruption or generation of key HR intermediates.

Materials and Methods

Stopped-flow measurements were carried out in SF50 buffer [50 mM Tris-HCl (pH 7.5), 50 mM NaCl, 1 mM DTT, 5 mM MgCl₂] at 25 °C in KinTek SF-2004 and BioLogic SFM 300 instruments. Postmixing concentrations are stated in all experiments. P_i liberation from ATP was followed using a fluorescently labeled P_i binding protein (MDCC-PBP) (51). MDCC-PBP calibration and single-round translocation experiments were performed as described earlier (15, 27), except that the protein trap was DxSO₄. Trp fluorescence was detected through a 320-nm cutoff filter at 280-nm excitation at a 4-nm slit width. DNA concentrations

are expressed as those of oligonucleotide and polynucleotide molecules (as opposed to constituent nucleotide units) if not otherwise indicated. Steady-state ATPase experiments were carried out in SF50 buffer plus 50 µg/mL BSA using a PK-LDH linked assay (14 U/mL PK, 20 U/mL LDH, 1 mM ATP, 1 mM phosphoenol pyruvate, 200 µM NADH) at 25 °C. Time courses of NADH absorbance ($\epsilon_{340} = 6,220 \text{ M}^{-1} \cdot \text{cm}^{-1}$) were followed in a Shimadzu UV-2101PC spectrophotometer. Additional descriptions of materials and methods and equations used in fits are provided in *SI Materials and Methods*.

1. Khakhar RR, Cobb JA, Bjergbaek L, Hickson ID, Gasser SM (2003) RecQ helicases: Multiple roles in genome maintenance. *Trends Cell Biol* 13:493–501.
2. Harmon FG, Kowalczykowski SC (1998) RecQ helicase, in concert with RecA and SSB proteins, initiates and disrupts DNA recombination. *Genes Dev* 12:1134–1144.
3. Bachrati CZ, Hickson ID (2008) RecQ helicases: Guardian angels of the DNA replication fork. *Chromosoma* 117:219–233.
4. Wu L, Hickson ID (2006) DNA helicases required for homologous recombination and repair of damaged replication forks. *Annu Rev Genet* 40:279–306.
5. Singleton MR, Dillingham MS, Wigley DB (2007) Structure and mechanism of helicases and nucleic acid translocases. *Annu Rev Biochem* 76:23–50.
6. Oh SD, et al. (2007) BLM ortholog, Sgs1, prevents aberrant crossing-over by suppressing formation of multichromatid joint molecules. *Cell* 130:259–272.
7. Bohr VA (2008) Rising from the RecQ-age: The role of human RecQ helicases in genome maintenance. *Trends Biochem Sci* 33:609–620.
8. Harrigan JA, Bohr VA (2003) Human diseases deficient in RecQ helicases. *Biochimie* 85: 1185–1193.
9. Hanada K, et al. (1997) RecQ DNA helicase is a suppressor of illegitimate recombination in *Escherichia coli*. *Proc Natl Acad Sci USA* 94:3860–3865.
10. Handa N, Morimatsu K, Lovett ST, Kowalczykowski SC (2009) Reconstitution of initial steps of dsDNA break repair by the RecF pathway of *E. coli*. *Genes Dev* 23:1234–1245.
11. Courcelle J, Hanawalt PC (1999) RecQ and RecJ process blocked replication forks prior to the resumption of replication in UV-irradiated *Escherichia coli*. *Mol Gen Genet* 262: 543–551.
12. Velankar SS, Soultanas P, Dillingham MS, Subramanya HS, Wigley DB (1999) Crystal structures of complexes of PcrA DNA helicase with a DNA substrate indicate an inchworm mechanism. *Cell* 97:75–84.
13. Dillingham MS, Wigley DB, Webb MR (2000) Demonstration of unidirectional single-stranded DNA translocation by PcrA helicase: Measurement of step size and translocation speed. *Biochemistry* 39:205–212.
14. Lee JY, Yang W (2006) UvrD helicase unwinds DNA one base pair at a time by a two-part power stroke. *Cell* 127:1349–1360.
15. Gyimesi M, Sarlós K, Kovács M (2010) Processive translocation mechanism of the human Bloom's syndrome helicase along single-stranded DNA. *Nucleic Acids Res* 38: 4404–4414.
16. Tomko EJ, Fischer CJ, Niedziela-Majka A, Lohman TM (2007) A nonuniform stepping mechanism for *E. coli* UvrD monomer translocation along single-stranded DNA. *Mol Cell* 26:335–347.
17. Dumont S, et al. (2006) RNA translocation and unwinding mechanism of HCV NS3 helicase and its coordination by ATP. *Nature* 439:105–108.
18. Lucius AL, Lohman TM (2004) Effects of temperature and ATP on the kinetic mechanism and kinetic step-size for *E. coli* RecBCD helicase-catalyzed DNA unwinding. *J Mol Biol* 339:751–771.
19. Levin MK, Gurjar M, Patel SS (2005) A Brownian motor mechanism of translocation and strand separation by hepatitis C virus helicase. *Nat Struct Mol Biol* 12:429–435.
20. Umezu K, Nakayama H (1993) RecQ DNA helicase of *Escherichia coli*. Characterization of the helix-unwinding activity with emphasis on the effect of single-stranded DNA-binding protein. *J Mol Biol* 230:1145–1150.
21. Dou SX, Wang PY, Xu HQ, Xi XG (2004) The DNA binding properties of the *Escherichia coli* RecQ helicase. *J Biol Chem* 279:6354–6363.
22. Umezu K, Nakayama K, Nakayama H (1990) *Escherichia coli* RecQ protein is a DNA helicase. *Proc Natl Acad Sci USA* 87:5363–5367.
23. Harmon FG, Kowalczykowski SC (2001) Biochemical characterization of the DNA helicase activity of the *Escherichia coli* RecQ helicase. *J Biol Chem* 276:232–243.
24. Xu HQ, et al. (2003) The *Escherichia coli* RecQ helicase functions as a monomer. *J Biol Chem* 278:34925–34933.
25. Zhang XD, et al. (2006) *Escherichia coli* RecQ is a rapid, efficient, and monomeric helicase. *J Biol Chem* 281:12655–12663.
26. Li N, et al. (2010) Multiple *Escherichia coli* RecQ helicase monomers cooperate to unwind long DNA substrates: A fluorescence cross-correlation spectroscopy study. *J Biol Chem* 285:6922–6936.
27. Pan BY, et al. (2010) Mutual inhibition of RecQ molecules in DNA unwinding. *J Biol Chem* 285:15884–15893.
28. Bernstein DA, Zittel MC, Keck JL (2003) High-resolution structure of the *E. coli* RecQ helicase catalytic core. *EMBO J* 22:4910–4921.
29. Zittel MC, Keck JL (2005) Coupling DNA-binding and ATP hydrolysis in *Escherichia coli* RecQ: Role of a highly conserved aromatic-rich sequence. *Nucleic Acids Res* 33: 6982–6991.
30. Gyimesi M, Sarlós K, Derényi I, Kovács M (2010) Streamlined determination of processive run length and mechanochemical coupling of nucleic acid motor activities. *Nucleic Acids Res* 38:e102.
31. Fischer CJ, Lohman TM (2004) ATP-dependent translocation of proteins along single-stranded DNA: Models and methods of analysis of pre-steady state kinetics. *J Mol Biol* 344:1265–1286.
32. Young MC, Kuhl SB, von Hippel PH (1994) Kinetic theory of ATP-driven translocases on one-dimensional polymer lattices. *J Mol Biol* 235:1436–1446.
33. Fischer CJ, Yamada K, Fitzgerald DJ (2009) Kinetic mechanism for single-stranded DNA binding and translocation by *Saccharomyces cerevisiae* Isw2. *Biochemistry* 48: 2960–2968.
34. Fischer CJ, Maluf NK, Lohman TM (2004) Mechanism of ATP-dependent translocation of *E. coli* UvrD monomers along single-stranded DNA. *J Mol Biol* 344:1287–1309.
35. Rajagopal V, Gurjar M, Levin MK, Patel SS (2010) The protease domain increases the translocation stepping efficiency of the hepatitis C virus NS3-4A helicase. *J Biol Chem* 285:17821–17832.
36. Bianco PR, et al. (2001) Processive translocation and DNA unwinding by individual RecBCD enzyme molecules. *Nature* 409:374–378.
37. Matlock DL, et al. (2010) Investigation of translocation, DNA unwinding, and protein displacement by NS3h, the helicase domain from the hepatitis C virus helicase. *Biochemistry* 49:2097–2109.
38. Niedziela-Majka A, Chesnik MA, Tomko EJ, Lohman TM (2007) *Bacillus stearothermophilus* PcrA monomer is a single-stranded DNA translocase but not a processive helicase in vitro. *J Biol Chem* 282:27076–27085.
39. Manosas M, Xi XG, Bensimon D, Croquette V (2010) Active and passive mechanisms of helicases. *Nucleic Acids Res* 38:5518–5526.
40. Ali JA, Maluf NK, Lohman TM (1999) An oligomeric form of *E. coli* UvrD is required for optimal helicase activity. *J Mol Biol* 293:815–834.
41. Maluf NK, Fischer CJ, Lohman TM (2003) A Dimer of *Escherichia coli* UvrD is the active form of the helicase in vitro. *J Mol Biol* 325:913–935.
42. Maluf NK, Ali JA, Lohman TM (2003) Kinetic mechanism for formation of the active, dimeric UvrD helicase-DNA complex. *J Biol Chem* 278:31930–31940.
43. Cheng W, Hsieh J, Brendza KM, Lohman TM (2001) *E. coli* Rep oligomers are required to initiate DNA unwinding in vitro. *J Mol Biol* 310:327–350.
44. Brendza KM, et al. (2005) Autoinhibition of *Escherichia coli* Rep monomer helicase activity by its 2B subdomain. *Proc Natl Acad Sci USA* 102:10076–10081.
45. Compton SA, Tolun G, Kamath-Loeb AS, Loeb LA, Griffith JD (2008) The Werner syndrome protein binds replication fork and Holliday junction DNAs as an oligomer. *J Biol Chem* 283:24478–24483.
46. Muzzolini L, et al. (2007) Different quaternary structures of human RECQL are associated with its dual enzymatic activity. *PLoS Biol* 5:e20.
47. Vindigni A, Hickson ID (2009) RecQ helicases: Multiple structures for multiple functions? *Hfsp J* 3:153–164.
48. Rad B, Kowalczykowski SC (2012) Efficient coupling of ATP hydrolysis to translocation by RecQ helicase. *Proc Natl Acad Sci USA* 109:1443–1448.
49. Rad B, Kowalczykowski SC (2012) Translocation of *E. coli* RecQ helicase on single-stranded DNA. *Biochemistry* 51:2921–2929.
50. Hickson ID, Mankouri HW (2011) Processing of homologous recombination repair intermediates by the Sgs1-Top3-Rmi1 and Mus81-Mms4 complexes. *Cell Cycle* 10: 3078–3085.
51. Brune M, Hunter JL, Corrie JE, Webb MR (1994) Direct, real-time measurement of rapid inorganic phosphate release using a novel fluorescent probe and its application to actomyosin subfragment 1 ATPase. *Biochemistry* 33:8262–8271.